Original Article

JOURNAL OF REINFORCED PLASTICS & COMPOSITES

Journal of Reinforced Plastics and Composites
2015, Vol. 34(2) 116–130
© The Author(s) 2014
Reprints and permissions:
sagepub.co.uk/journalsPermissions.nav
DOI: 10.1177/0731684414565225
jrp.sagepub.com
SAGE

Influence of thermo-oxidative aging on the impact property of conventional and graphene-based carbon fabric composites

Wei Fan, Jia-lu Li, Huan Wang and Dan-dan Guo

Abstract

The effects of reinforced structure (three-dimensional braided preform and laminated plain woven fabric) and graphene nanoplatelet-reinforced hierarchical interface on the impact properties of carbon fabric composites after thermo-oxidative aging were investigated. The results indicated that the impact properties decreased with increasing aging time due to the degradation of the matrix and fiber–matrix interface. After exposure to 140°C for 1200 h, the peak impact force and impact strength retention rates of 3D-braided graphene nanoplatelet-coated carbon fiber-reinforced composite were 13% and 8% higher than those of the laminated composite, respectively. One of the reasons was the graphene nanoplatelet-reinforced gradient interphase may provide an effective shield against interface oxidation, transfer the localized thermal stress, and restrict the movement of the different phase of the materials at the composites interface. Another reason was the integrated structure of the 3D-braided composite can make the fiber bear impact force together although the resin was damaged and the adhesive force between fiber bundles and resin decreased after thermo-oxidative aging. This synergetic reinforcing effect of 3D-braided structure and graphene nanoplatelet-reinforced hierarchical interface provides an easy and effective way to design and improve the thermo-oxidative stability of carbon fiber-reinforced composites.

Keywords

Polymer matrix composites, thermo-oxidative aging, reinforced structure, graphene, mechanical property, interface

www.spm.com.cn

Introduction

Carbon fiber polymer matrix composites (CFPMCs) have been widely used in aerospace structures due to their superior specific strength and stiffness.[1–3] In aerospace structures, some composite parts adjacent to a hot air source are long exposed to rather severe thermal conditions.[4] Under such conditions, oxidation reaction–diffusion phenomena take place within CFPMCs, introducing damage at the fiber–matrix interfaces and causing formation of matrix microcracks.[5] However, unfortunately, the composite structures used in aerospace are prone to be subjected to low-velocity impact,[6] which is sensitive to interface performance.[7] Therefore, the matrix transverse cracking and fiber–matrix interface debonding of CFPMCs caused by thermo-oxidative aging will bring great safety hidden trouble for their following use.

For the conventional laminated composites, the occurrence and the development of microscopic damage (fiber–matrix debonding or micro-cracks) give rise to the onset of oxidized–damaged layers that propagates along the composite plies. This process is prone to drilling-induced delamination damage. By contrast, three-dimensional (3D)-braided composites show low delamination tendency in combination with near net shape manufacturing, out-of-plane stiffness, high strength and impact tolerance as well as anti-ablation resistance.[8] However, no studies have focused on the impact property of 3D-braided composites after

Composite Research Institute of Tianjin Polytechnic University, Tianjin and Education Ministry Key Laboratory of Advanced Textile Composite Materials, Tianjin, China

Corresponding author:
Jia-lu Li, Composite Research Institute of Tianjin Polytechnic University, Tianjin and Education Ministry Key Laboratory of Advanced Textile Composite Materials, Tianjin 300387, China.
Email: lijialu@tjpu.edu.cn

thermo-oxidative aging. Therefore, we do not know whether the advantages of 3D braided composites could help to improve the thermo-oxidative stability of CFPMCs.

Previous research[9] has shown that good interfacial properties can improve the thermo-oxidative stability of CFPMCs. In recent years, the introduction of graphene nanoplatelet (GN) into conventional continuous fiber-reinforced polymer composites to create hierarchical reinforcement structures is a topic of significant current interest due to the unique structures, outstanding strength and modulus, excellent electrical and thermal properties of the GN.[1,10] It has been demonstrated that by adopting the GN, significant improvements are achieved in CFPMCs, especially for the fiber–matrix interphase and matrix-dominated out-of-plane performances, such as interfacial shear strength,[1,11] impact strength,[1] fatigue resistance.[10] However, there are few studies regarding the properties of GN-reinforced CFPMCs after thermo-oxidative aging.

For this investigation, the purpose of the current investigation was to determine the role of reinforced structure (3D and four-directional (4Dir) braiding preform and laminated plain woven fabric) and GN-reinforced hierarchical interface on the impact property of CFPMCs after thermo-oxidative aging. Therefore, specimens were thermally oxidized at 140°C for various durations. After exposure to the high temperature, composites are characterized to (1) determine the weight loss and impact property at different exposure times; (2) identify the failure modes of the 3D-4Dir braided composites and laminated composites, and observe the corresponding micro-cracks and surface damage; and (3) understand the reinforced mechanism using the different reinforced structure and the GN-reinforced hierarchical interface.

Experimental details

Materials

Commercially available, T700-12 K carbon fibers (Toray) and plain woven T700-12 K carbon fiber fabric with areal density of 400 g/m^2 and warp and weft densities of 2.5 yarns/cm (Yi Xing new carbon fiber weaving co., Ltd) were used for this study. An epoxy resin JC-02 A based on diglycidyl ether of bisphenol A (Changshu Jaffa Chemical Co., Ltd.) with hardener JC-02B (improved methyl tetrahydrophthalic anhydride) and accelerant JC-02 C (tertiary amine) was used as matrix. Graphite powders with an average diameter of 10 μm were purchased from Qingdao AoKe ShiMoCo. Ltd., China. Concentrated H_2SO_4 (98%), concentrated H_3PO_4 (85%), $KMNO_4$, acetone, and 30% H_2O_2 (Tianjin Feng Chuan Co., Ltd.) were used to make GN.

Preparation of GN

Graphite oxide (GO) was synthesized with a Marciano's method.[12,13] A 9:1 mixture of concentrated H_2SO_4/H_3PO_4 (360:40 ml) was added to a mixture of graphite powders (3.0 g, 1 wt equiv) and $KMnO_4$ (18.0 g, 6 wt equiv), producing a slight exotherm to 35–40°C. The mixture was stirred for 12 h at 50°C, forming a thick paste. Subsequently, it was cooled to room temperature and poured onto ice (400 ml) with 30% H_2O_2 (3 ml). The remaining solid materials were then washed in succession with deionized water until the pH was 7. At last, they were dried at vacuum freeze drier for 12 h to get GO. The dry GO was grinded into powder. GN was produced by the thermal exfoliation[10] of GO. The GO powder was placed (200 mg) in a quartz boat and the quartz boat was put carefully into the vacuum–atmosphere tube furnace (SK-1400°C, Central laboratory electric furnace co., LTD. Tianjin, China) preheated to 1050°C and held in the furnace for ~35 s. When the quartz boat was taken out, the black flocculent material was the GN.

Preparation of GN-coated fibers

The GN was dispersed in acetone, and sonicated for 2 h to obtain the stable suspension of 1 mg ml^{-1}. After that, the T700-12 K carbon fibers that had been weighed were soaked in the homogeneous mixtures for 20 s to absorb the solutions containing GN. Then these carbon fibers coated by GN were dried at 50°C under vacuum and the weight of carbon fibers was measured again. The weight of GN was calculated by changes in weight of carbon fibers. Then these steps were repeated until the contents of GN in composites reached 1 wt%. The weight of GN in the composite was chosen as 1% because our previous work has proved that this content was the best proportion to improve the bending and shear properties of carbon fiber/epoxy composites at the room temperature.[14] The procedure of production of the GN-coated fibers is illustrated in Figure 1.

Preparation of 3D-4Dir braided carbon fiber/epoxy composites (BC), 3D-4Dir braided GN-coated carbon fibers/epoxy composites (BGC), laminated plain woven carbon fiber/epoxy composites (LC) and neat resin (NR)

Both the 3D-4Dir braided virgin carbon fiber preforms and 3D-4Dir braided GN-coated carbon fibers preforms were manufactured by the intertwining or orthogonal interlacing of four sets of yarns braiders

www.sim.com.cn

to form a 3D sheet fabric.[15] The 3D-4Dir braided architecture is illustrated in Figure 2(c). It is characterized by almost all the braider yarns being offset at different angles between the in-plane and through-thickness directions, which can be seen clearly from the tracer yarn (colored yarns). An idealized model of the braid preform surface is shown in Figure 2(e), where h is the braiding pitch length, θ is the surface braiding angle, and α is the braiding angle. The average braiding angle α of 3D-4Dir-braided preforms in this article was 22.3°. The laminated plain woven fabric is illustrated in Figure 2(d). The production process of BGC was the same as that of the BC, the difference between them was that the fibers used for BC were virgin carbon fibers (Figure 2(b)) and those used for BGC were the GN-coated carbon fibers (Figure 2(a)). The making process of the composites and the neat resin is covered elsewhere.[16] The final specimens of the BGC, BC, and LC are illustrated in Figure 2(f), 2(g), and 2(j), respectively. The fiber volume fractions for the three composites were about 55%.

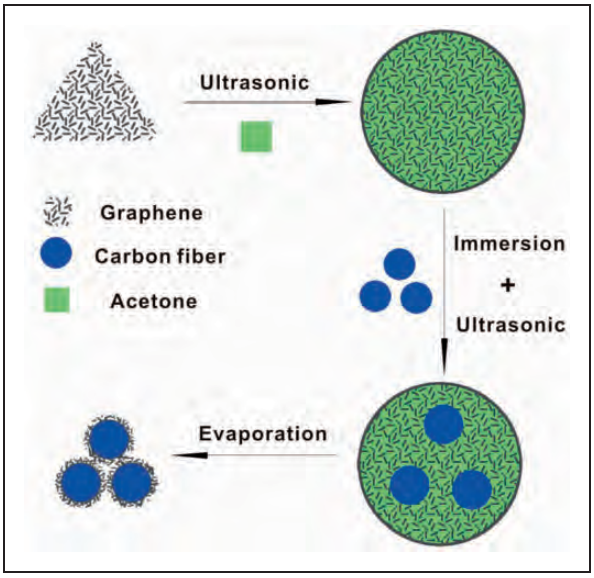

Figure 1. Schematic of the graphene-depositing process on carbon fibers.

Accelerated aging experiments

In order to evaluate the durability of the composites, an accelerated thermo-oxidative aging procedure was adopted. Specimens were isothermally aged at 140°C for 168, 360, 720, and 1200 h. After heating and at a given aged time, specimens were removed, cooled in a desiccator to avoid the humidity absorption. The specimens were stored at 25 ± 3°C for at least 24 h prior to test.

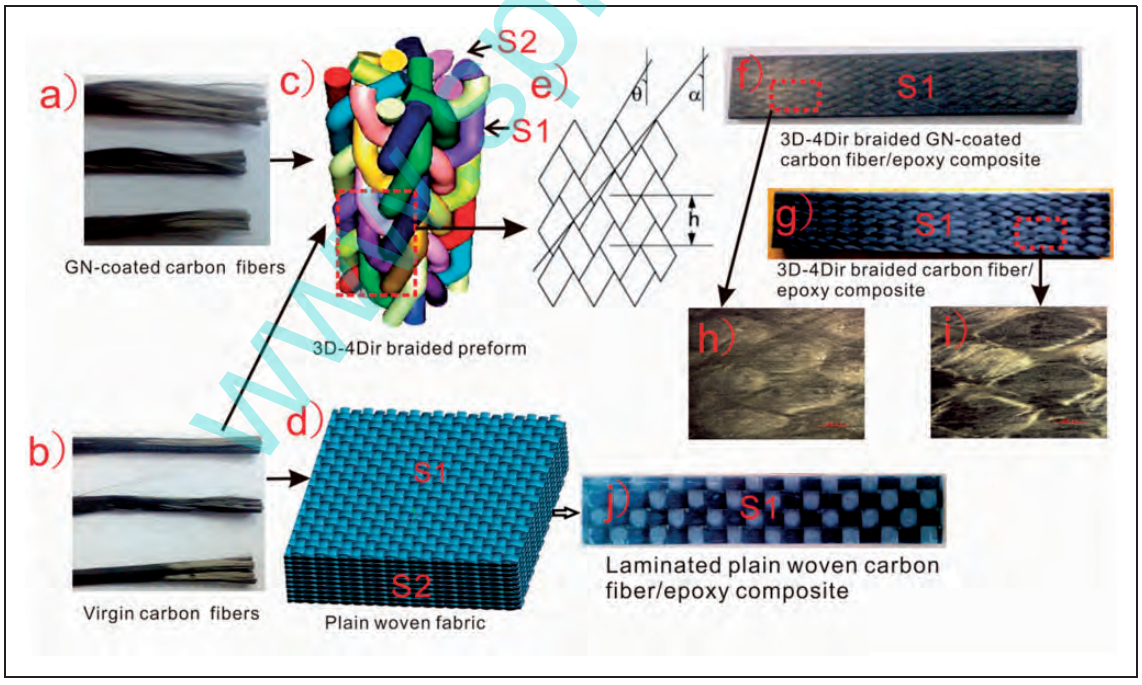

Figure 2. GN-coated carbon fibers (a); virgin carbon fibers (b); the reinforced structure diagram of BC (c); the reinforced structure diagram of LC (d); an idealized model of the 3D-4Dir braided preform surface (e); an impact specimen of BGC (f), BC (g) and LC (j); (h) zoom on the specimen surface corresponding to (f); (i) zoom on the specimen surface corresponding to (g); S_1 = area of nonmachined resin-rich surfaces and S_2 = area of surfaces cut perpendicular to fibers.

www.sagepub.com.cn

Tests

The surface topography of carbon fibers and cross-section of composite specimens were obtained on a Hitachi S-4800 FE-SEM (field emission scanning electron microscope) and a VHX-1000 3D microscopy system. Atomic force microscopy (AFM) observation of the composites was performed on a CSPM 5500 scanning probe microscope. A JEOL TM-100 SEM was employed to observe fiber–matrix interfaces of the composites.

Thermal conductivity of the composites was examined by TC 3010 apparatus (Xi'an Xiatech Electronic Technology Co. Ltd., China) according to ASTM C1113/C1113M-09. The testing specimens had dimensions of 40 mm × 30 mm × 4 mm.

Dynamic mechanical analysis was conducted on the specimens to investigate the glass transition temperature (T_g) according to ASTM E1640-2009 with a three-point bending mode. The tests were performed in the scanning temperature mode, in the range from 40°C to 185°C, at a heating rate of 5°C/min, and with an oscillating frequency of 1.0 Hz. Three specimens of rectangle shape with a nominal size of 60 mm × 10 mm × 2 mm were analyzed for each level of thermal treatment.

An electronic balance with 0.1 mg accuracy was used for recording the weight loss of composites. The impact tests were conducted in accordance with GB/T 1451–2005 with a three-point loading method with a 70 mm span between the supports. The impact tests were measured by Instron Dynatup 9250 HV (Figure 3), using an impact mass of 5.5 kg and a wedge-shaped impactor. The drop height was adjusted to produce an impact velocity of approximately 2 m/s. The dimensions of the specimens (five for each condition) for impact tests were 120 mm × 15 mm × 4 mm.

Results and discussion

Surface topography and stiffness distribution of the hierarchical interphase

To verify the introduction of hierarchical layer, the interfacial phase structures of the pristine and the multi-scale composites loading with 1 wt% GN were detected in detail. Surface morphologies of carbon

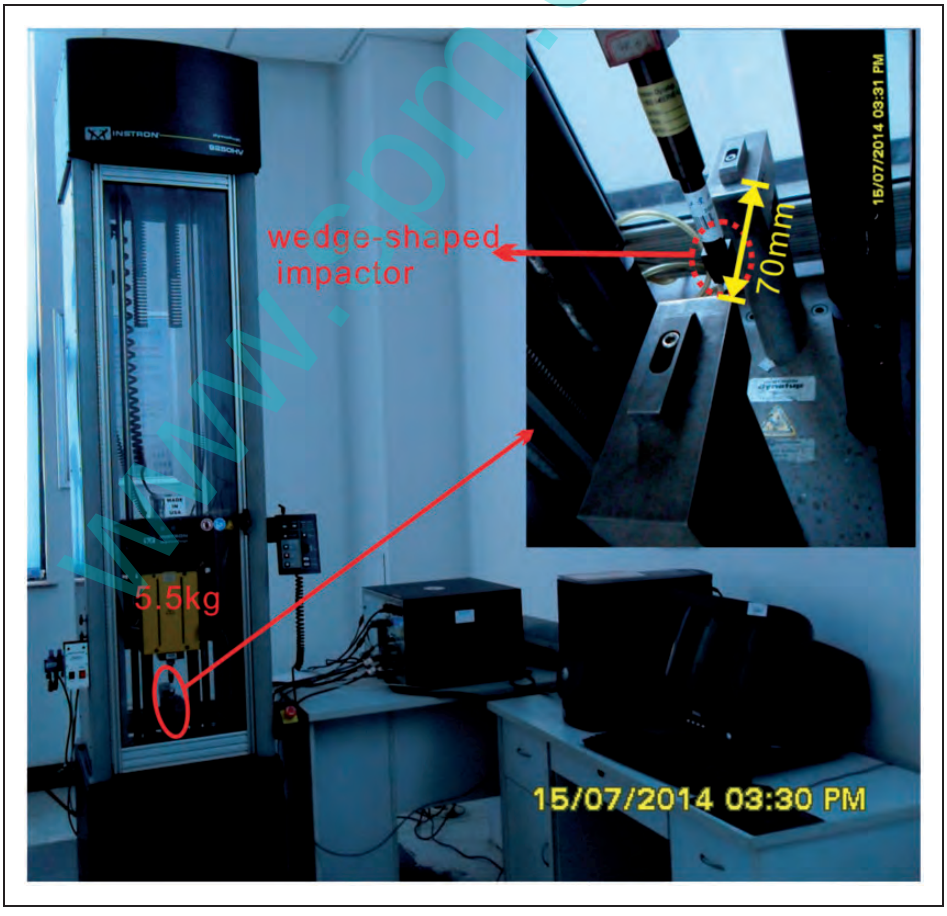

Figure 3. Drop-weight impact test setup (Instron Dynatup 9250 HV).

www.com.cn

fiber before and after depositing GN observed by FE-SEM are shown in Figures 4(a) and 5(a), respectively. It can be seen that the virgin T700 carbon fiber had a smooth surface. After absorbing GN, we can see that most GN were attached to the fiber surface (Figure 5(a)), which identified that a new hierarchical structure was formed.[17] Figures 4(b) and 5(b) are the schematic representations of the unit cell that constitutes the two-phase (carbon fiber/epoxy) composite (BC) and the three-phase (carbon fiber/graphene/epoxy) hierarchical composite (BGC), respectively. Linear scanning system of FE-SEM is used to evaluate the element distribution in interface region and the results are shown in Figures 4 and 5. As illustrated in Figure 4(d), a sudden drop in the amount of carbon element can be observed from fiber to matrix. However, this drop tendency became much slower after addition of GN (Figure 5(d)), which demonstrated the formation of nanocomposite interface layer reinforced by GN in the carbon fiber–epoxy interfacial phase. In addition, carbon element content dwindled steadily from carbon fibers to epoxy, which indicated the gradient distribution of GN in the BGC and supported the construction of gradient interface layers with a thickness of ~0.98 μm (Figure 5(d)).

For further investigation of the interfacial phase structures of composites, the force modulation mode of AFM is adopted to study the stiffness of various phases of composites, which allowed a qualitative statement about the local modulus of specimen surface using an oscillating cantilever tip that indents into the specimen surface. The corresponding cantilever amplitude will change under scanning in accordance with the local modulus of specimen. The indentation will be larger on compliant areas, while smaller on stiff areas of the specimen. Thus, different response of the cantilever from areas with different modulus could be observed.[18,19] However, due to the fact that only two external channels are at our disposal, only the amplitude of the electrical AC current signal and the amplitude of the mechanical AC signal can be recorded.[19] Therefore, the relative stiffness value was indirectly indicated by the voltage generated from the cantilever deflection of AFM. Figures 4(e) and 5(e) showed the relative stiffness images of cross-section areas in BC and BGC, respectively. The relative stiffness image of carbon fibers was brighter than the surrounding epoxy, which meant that the stiffness of carbon fibers was higher than epoxy. Besides, it demonstrated that the

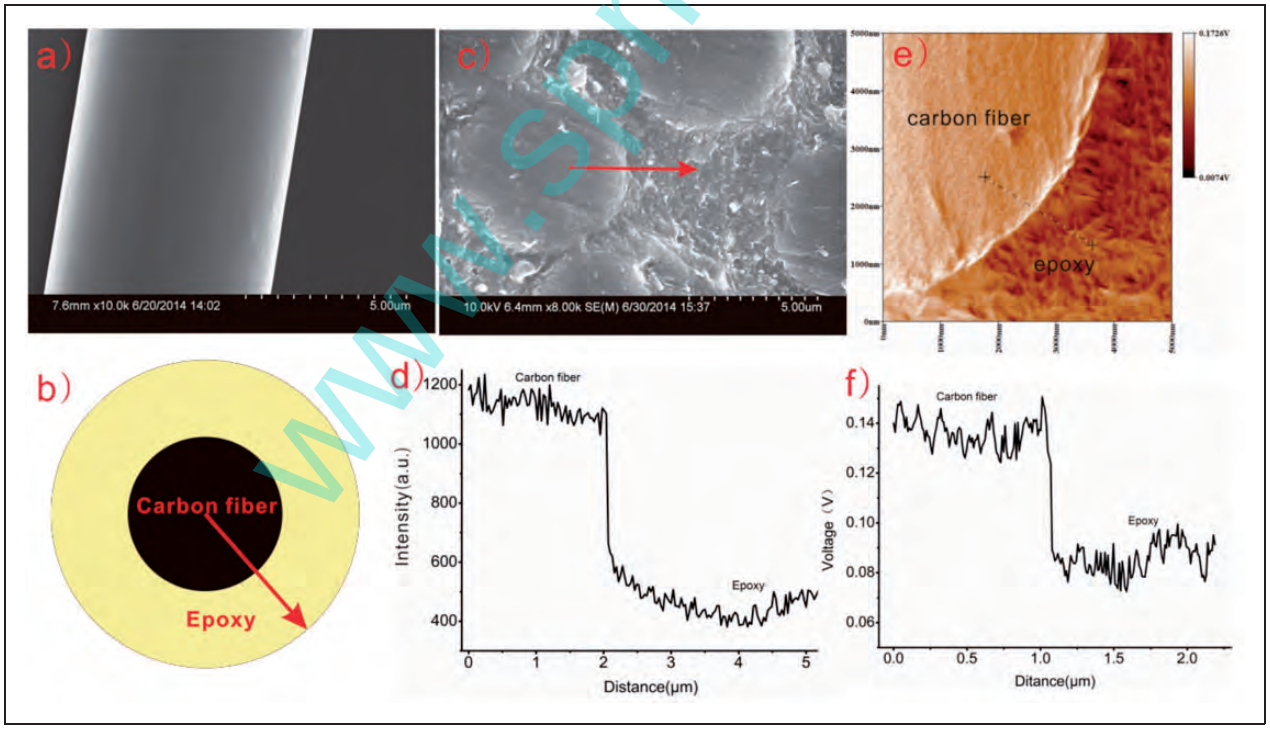

Figure 4. (a) the surface morphologies of the raw carbon fibers; (b) schematic representation of the unit cell that constitutes the two-phase (carbon fiber/epoxy) composite (BC); (c) FE-SEM image of cross-section of the BC; (d) carbon element content varying from carbon fibers to epoxy along the direction of arrow in (c); (e) relative stiffness image of cross-section areas of the BC; (f) relative stiffness distribution curve of cross-section areas of the BC corresponding to (e).

www.spm.com.cn

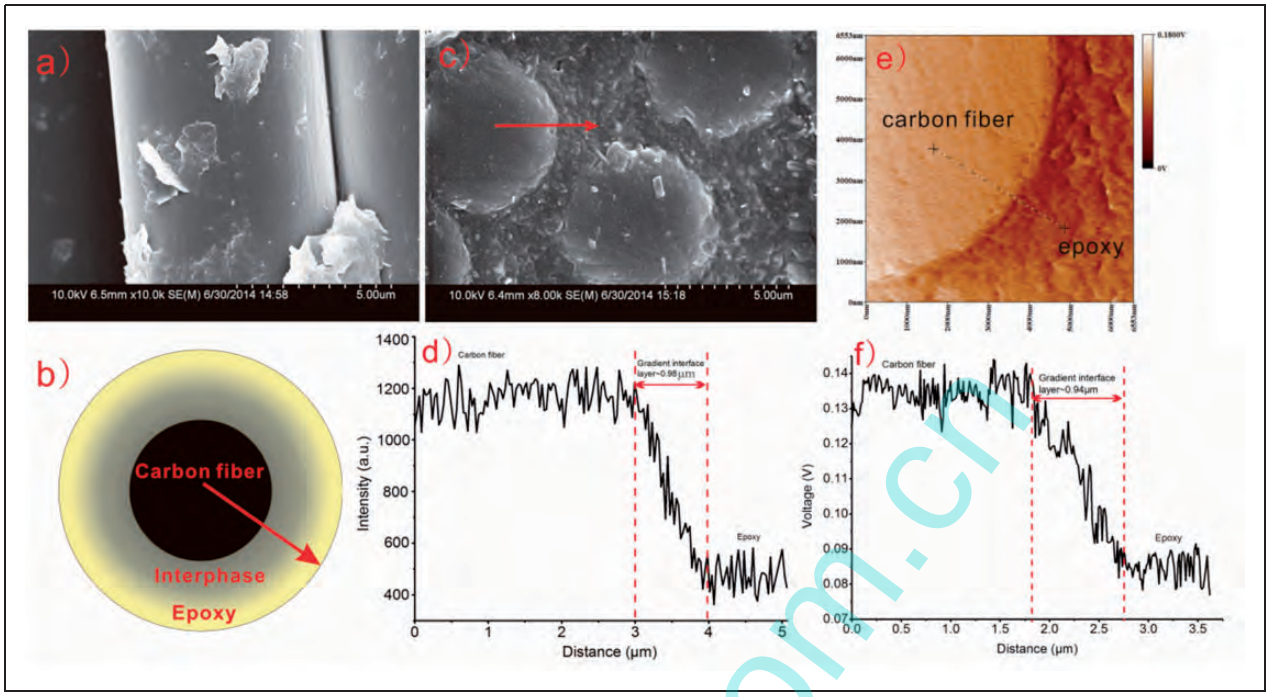

Figure 5. (a) the surface morphologies of the graphene-coated carbon fiber; (b) schematic representation of the unit cell that constitutes the three-phase (carbon fiber/graphene/epoxy) hierarchical composite (BGC); (c) FE-SEM image of cross-section of the BGC; (d) carbon element content varying from carbon fibers to epoxy along the direction of arrow in (c); (e) relative stiffness image of cross-section areas of the BGC; (f) relative stiffness distribution curve of cross-section areas of the BGC corresponding to (e).

relative stiffness image displayed a clear distinction between carbon fiber and the surrounding epoxy (Figure 4(e)). After incorporation of GN, the boundary of carbon fiber and epoxy became blurrier (Figure 5(e)). Figures 4(f) and 5(f) were the corresponding relative stiffness distribution curves of cross-section areas of Figures 4(e) and 5(e), respectively. There was a sharp drop of the stiffness from carbon fiber to epoxy for the BC (Figure 4(f)). Nevertheless, this drop became more gradual after adding GN, which implied the introduction of gradient interface layer and was in good agreement with the linear FE-SEM results. The interphase thickness value was ~0.94 μm in Figure 5(f), which was a little smaller than that in Figure 5(d) due to disparity of specimens and experimental errors.

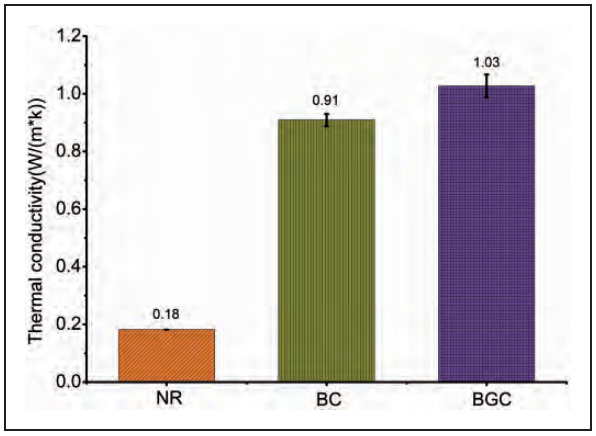

Figure 6. Thermal conductivity of NR, BC, and BGC.

Thermal conductivity analysis

Figure 6 shows that the thermal conductivity of the NR, BC, and BGC was 0.18, 0.91, and 1.03 W/(mk), respectively. It should be noted that the thermal conductivity of the BC and BGC in this paper was along the width of the specimens (transverse thermal conductivity of the composites). Compared with BC, the thermal conductivity of BGC was improved by 13% due to the small addition of GN (1 wt%) with high thermal conductivity (5000 W/(mk)).[20]

Thermomechanical analysis

The temperature corresponding to the peak maximum of loss modulus was defined as T_g, where the polymer material undergoes the maximum change in mobility of the polymer chains.[21] The T_g for NR (125.5°C) was smaller than for LC (127.6°C) and BC (141.9°C) despite the same cure cycles (Figure 7), which might be because the presence of fiber in the composites blocked the mobility of the polymer chains, causing the composites

www.sgm.com.cn

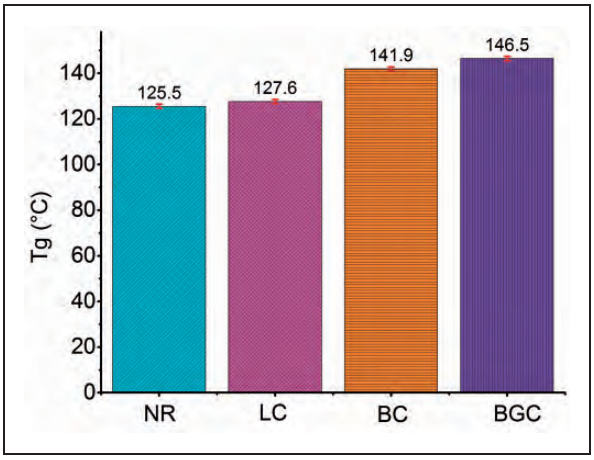

Figure 7. The T_g of the neat resin and the three composites.

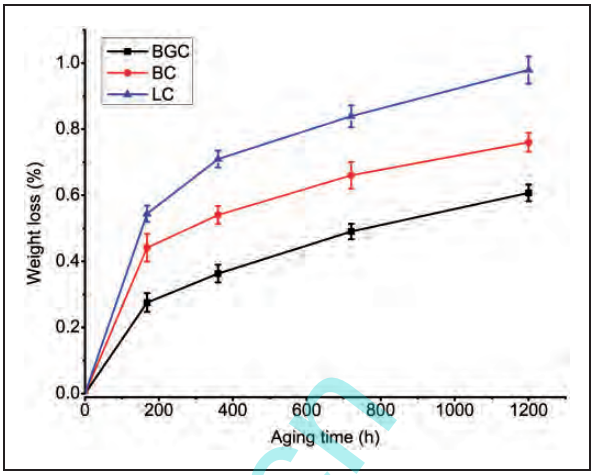

Figure 8. Weight loss vs. aging time for specimens aged at 140°C.

to have higher T_g. The T_g of BC was 14°C higher than that of LC, which might be related to the fact that the 3D-4Dir braided preform had more fiber-crossing points than that of plain woven fabric (Figure 2(c) and (d)). And the fiber-crossing points might hinder the flow of the molecules. The T_g of the BGC (146.5°C) was about 5°C higher than that of BC, which might be because of the rough and wrinkled surface topology of GN-modified carbon fiber (Figure 5(a)) which can enable it to mechanically interlock, increasing the interfacial friction and restricting the movement of the different phase of the materials at the composites interface.[18]

Weight loss analysis

Figure 8 illustrates the measured weight loss of the three composites at 140°C as a function of aging time. The present data were an average values obtained from the impact specimens. The weight loss increased with longer aging times. The weight loss of LC was about 1.3 and 1.8 times as high as that of BC and BGC, respectively.

In the case of CFPMCs, weight loss is (in general) associated only with the polymer, as the reinforced carbon fibers are thermally stable at 140°C.[22] In this research, the LC and BC specimens had the same matrix resin content (45%), so they should have the same weight loss. The weight loss of the two composites did not appear to follow the expected behavior that the weight loss of BC should be equal to that of the LC, but rather LC lost considerably more weight than BC under the same aging conditions. It was because surfaces of specimens with different microstructural characteristics were expected to exhibit different oxidation behavior.[23] The cross-section photomicrographs of LC aged at 140°C for 1200 h compared to an unaged one are shown in Figure 9. No damage was observed on the surface of the unaged specimen (Figure 9(a)). However, a lot of micro-cracks appeared on the aged specimen (Figure 9(b)). The micro-cracks largely appeared on the fiber end areas and few on the areas parallel to the fibers (Figure 9(c) and (d)). It was because the propagation of the oxidation in the axial direction of fiber was dramatically greater than in the transverse direction.[23] Therefore, a specimen with higher percentage of fiber end area exposed to air is more susceptible to interface oxidation, resulting in more weight loss.[5,23] The weight loss data presented in this article were an average of the values obtained from the impact specimens, so the surface area ratio $S_2/(S_1 + S_2)$ for LC and BC was 23% and 2.6%, respectively. However, the plain weave fabric only had half of the fibers perpendicular to S_2, so the actual fiber end area ratio of LC was 11.5%, which was four times more than that of BC. Besides, the LC had plies of two different orientations as its immediate neighbors, which was prone to develop oxidation growth gradients across the ply interfaces because of the anisotropy of oxidation diffusion.[24] It can be clearly seen that some micro-cracks even seem to have developed into delamination (Figure 9(d)). The micro-cracks created additional permeation paths for oxygen to penetrate deep into the composite during the aging process, accelerating the oxidation weight loss rate of composites. Therefore, the LC lost much more weight than BC at the same aging conditions, and the gap was continued to be expanded with the increasing of aging time.

The BC and BGC had the same surface area ratio $S_2/(S_1 + S_2)$, however, the weight loss of BC was 1.4 times as high as that of BGC. Two reasons may account for this phenomenon. To begin with, the GN produced by thermal reduction of GO[25] might have

www.spm.com.cn

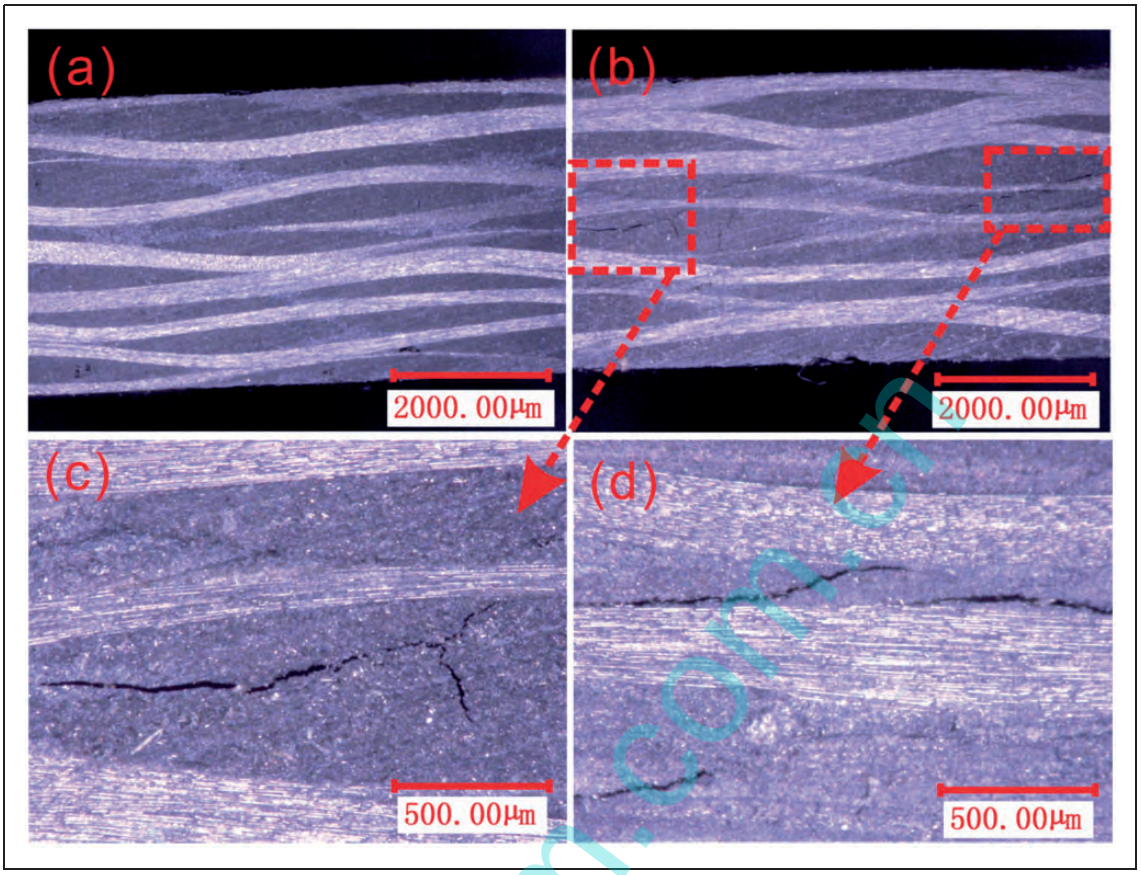

Figure 9. Photomicrographs of cross-section of (a) unaged and (b) aged (1200 h at 140°C) LC; zoom on thermo-oxidation-induced microcracks (c and d).

residual hydroxyl and epoxide functional groups, which could interact covalently with the epoxy chains thereby further promoting interfacial adhesion. A strong interface can hinder the diffusion of oxygen into the composites, reducing the oxidation weight loss of interface.[26] Secondly, the axial (100 W/(mk)) and radial thermal conductivity (11 W/(mk)) of T700 carbon fiber[27] was 555 and 61 times as high as those of NR (0.18 W/(mk)), respectively. Mismatches in the thermal conductivity between the fiber and matrix give rise to localized thermal stress at the fiber–matrix interface, which are prone to induce micro-cracks. After adding GN at the fiber–matrix interface in carbon fiber/epoxy composites, the thermal conductivity of BGC was improved by 13% compared to BC. The carbon element content dwindled steadily from carbon fibers to epoxy (Figure 5(d)) indirectly indicating that the thermal conductivity of the GN-reinforced gradient interphase layer was lower than that of carbon fiber and higher than that of matrix. The gradient conductive layer might transfer the interfacial thermal stress, mitigating the interface damage. The cross-section photomicrographs and SEM pictures of the fracture surfaces of the unaged and aged specimens in Figures 10 and 11 may be good evidences for the two points of views. It can be seen that no damage was observed on the unaged specimen surface (Figure 10(a)), but a lot of micro-cracks appeared on the end cross-section of the aged specimen (Figure 10(b)). The micro-cracks were also noted on the end cross-section of BGC (Figure 10(c)). However, in comparison to the BC, the extent of micro-cracks was much less in the BGC specimens. By comparing Figure 10(d) and (e), it can be seen that micro-cracks in BC were more open than in BGC, and the fiber–matrix debonding onset (Figure 10(d)) was observed clearly. Figure 11 shows the typical SEM pictures of the fracture surfaces of unaged and aged BC (left) and BGC (right). The fracture surfaces of LC were similar to those of BC, so the fracture surfaces of LC were not present in Figure 11. On fracture surfaces of both unaged specimens (Figure 11(a) and (f)), fibers were covered with the matrix representing a good adhesion of fiber and matrix. However, the adhesion of fiber and matrix on fracture surface of BGC seemed to be better than that of BC, which indicated that GN can promote

www.spm.com.cn

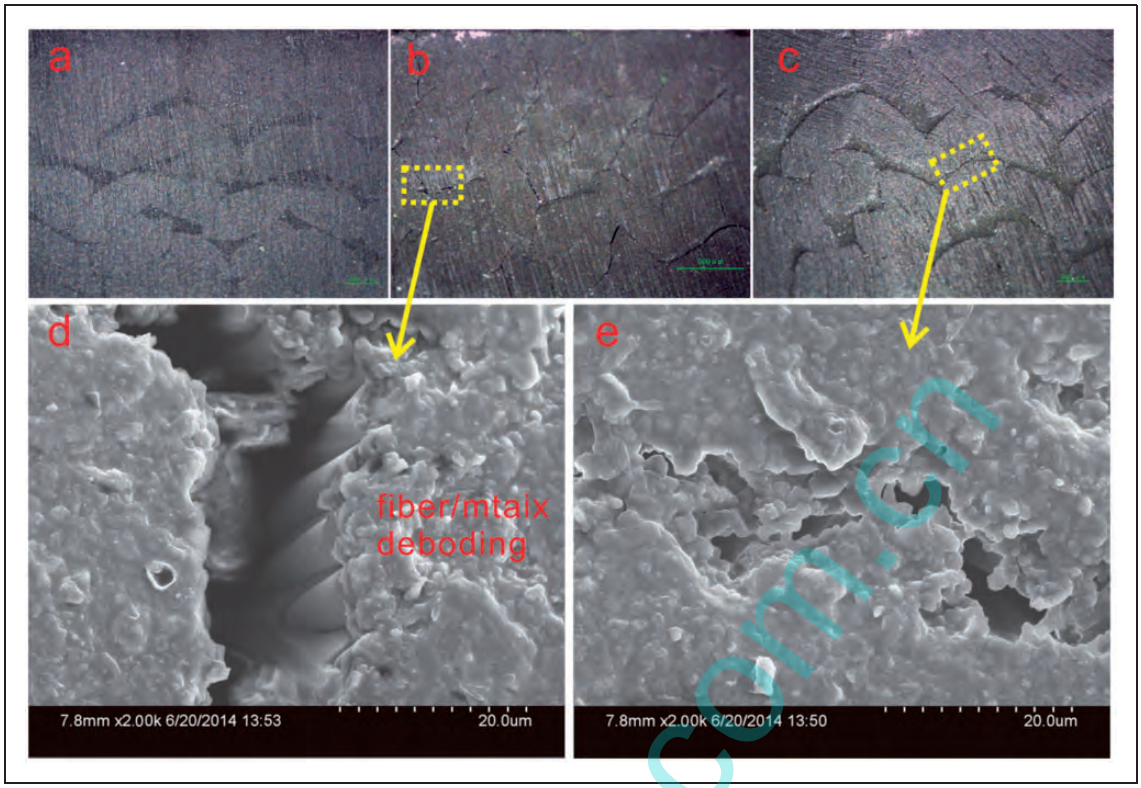

Figure 10. Photomicrographs of cross-sections of (a) unaged and aged (1200 h at 140°C) BC (b) and BGC (c); (d) zoom on thermo-oxidation-induced micro-cracks corresponding to (b); (e) zoom on thermo-oxidation-induced micro-cracks corresponding to (c).

interfacial adhesion. In aged BC specimens, the cracks propagated almost entirely along the fiber–matrix interface after aging time of 168 h (Figure 11(b)); resins attached to the fibers decreased and the grooves were formed due to the pull out of the fibers after aging time of 360 h (Figure 11(c)); with increase of aging time, the fibers were lying loosely and the fiber surfaces were completely devoid of matrix material (Figure 11(d) and (e)). Significant interfacial failure was also noted in the fracture surfaces of composites with GN-coated fibers. However, in comparison to the BC specimens, the extent of the interfacial failure was much less in the BGC specimens. The fibers on the fracture surfaces of BGC specimens were still held together by the matrix resin after aging time of 720 h (Figure 11(i)). Although the fibers were lying loosely after aging time of 1200 h (Figure 11(j)), the matrix resins were still present, filling the space between the fibers. The photomicrographs and SEM analyses illustrated that GN-reinforced gradient interphase layer in BGC not only can promote interfacial adhesion but also can transfer the interfacial thermal stress, mitigating the interface damage.

Impact properties analysis

Figure 12(a) and (b) shows the impact force-deflection and total energy-deflection traces of the three unaged composites, respectively. The impact force-deflection traces for both BC and BGC showed a typical brittle failure, where the force increased in an almost linear fashion until catastrophic failure occurred, at which point the force decreased instantaneously. After a brief fluctuation, the force decreased slowly. The impact force-deflection trace for LC also showed a typical brittle failure, but where the force increased in small saw-toothed fashion until catastrophic failure occurred, at which point the force decreased instantaneously. After drastic fluctuations, the force decreased in saw-toothed fashion until it fell to zero. Besides, the fracture deflection of LC was much larger than that of BC and BGC. The total energy-deflection traces for the three composites increased quickly at the beginning. After an obvious turning point corresponding to the sharp decrease in force-deflection trace, the energy increased to the peak values at a relative slow speed. The differences between the force-deflection traces for the three composites were related to their failure modes. Figure 13(a) and (b) shows the representative failure modes of unaged LC and BC specimens after impact test, respectively. The failure modes were similar for both BC and BGC, therefore, only one set of them was presented in Figure 13(b). From Figure 13(a), it can be seen that the fibers on the tension surface of LC fractured completely, only a very small amount of

www.spm.com.cn

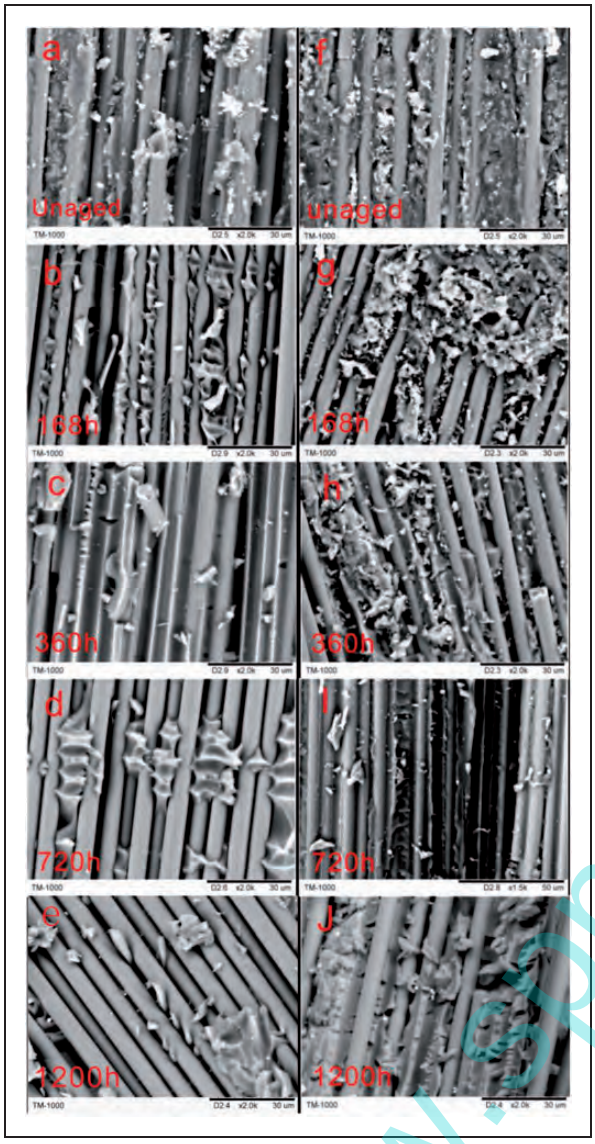

Figure 11. SEM pictures of the fracture surfaces of unaged and aged (1200 h at 140°C) BC (left) and BGC (right).

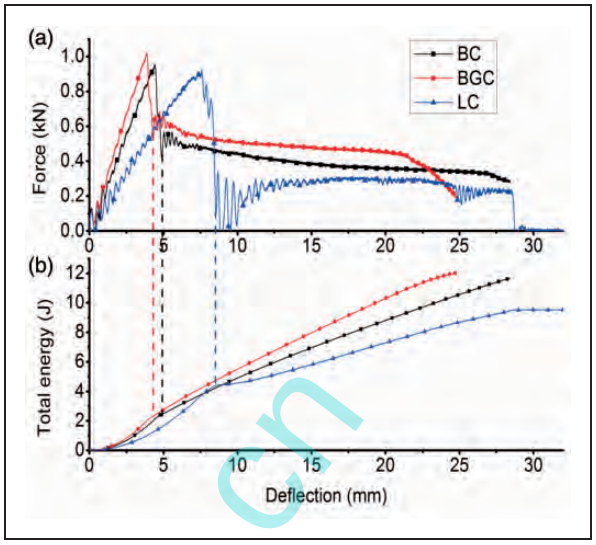

Figure 12. Typical force–deflection impact curves (a) and total energy-deflection curves (b) for the three unaged composites.

fibers exhibited bridging on the compression surface, and delamination can be seen clearly on the side surface. For BC (Figure 13(b)), no fibers fractured and only some resin became white on the tension surface, a few of fibers fractured and some resin were pushed out on the compression and side surfaces, but there was no delamination on the side surface. By comparing LC and BC, we can conclude that the saw-toothed wave on the force-deflection trace of LC was characteristic of delamination damage. As the BC and BGC damaged as a whole structure, there were no saw tooth waves on the force-deflection traces.

In order to avoid the effects of specimen size, the maximum peak impact force per cross-sectional area (F_{max}) was used for comparison. Figure 14(a) and (b) shows the F_{max} and impact strength for the three unaged composite specimens. From Figure 14(a), it can be seen that the F_{max} of LC, BC, and BGC was 14.7, 16.3, and 18.1 (MN/m^2), respectively. From Figure 14(b), it can be seen that the impact strength of LC, BC, and BGC was 104.8, 161.4, and 192.5 kJ/m^2, respectively. The F_{max} and impact strength of BC increased by 11% and 54%, respectively, compared with those of LC. This was related to the fact that the reinforced structures for BC and LC had different response to the impact load. Once a specimen surface was impacted by the impactor, it would produce compression stress waves perpendicular to the specimen surface, then the stress wave would propagate along the specimen thickness direction to the back of the specimen and finally be reflected to form the tensile stress. When the impact energy was big enough, the tensile stress would be turned into interlaminar stress. For LC, the delamination damage (the side surface in Figure 13(a)) happened following bending deformation when the interlaminar stress exceeded its interlaminar strength. With the increase of specimen deformation, the transverse shear force between the layers would promote interface cracks to extend, and then the impact load was quickly passed to fibers when the cracks extended to the interface of fiber and matrix. Under the tension stress, the fibers fractured (the tension surface in Figure 13(a)), finally lead to the complete break of the specimen (the load fell to zero, see Figure 12(a)). However, for the BC, the stress wave was hindered by the near net shape structure formed by the fiber and matrix when it propagated from the compression surface to the tension surface along the specimen thickness direction. Therefore, there were only a few of

www.sgm.com.cn

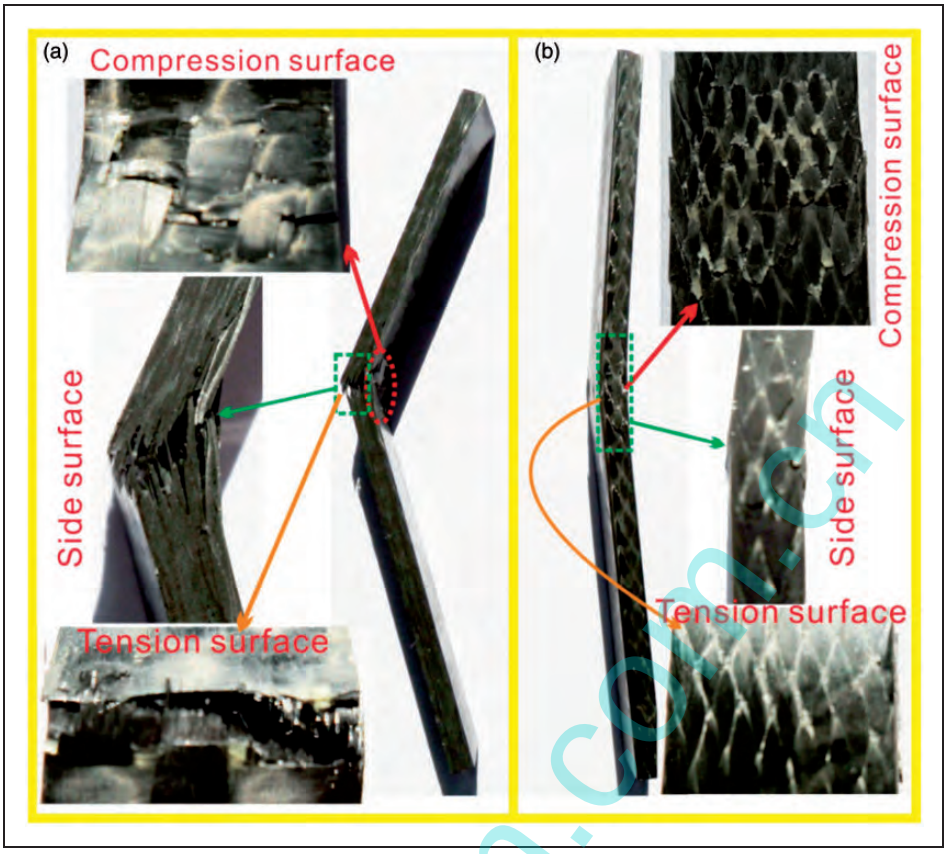

Figure 13. Representative failure modes of unaged LC (a) and BC (b) specimens after impact test.

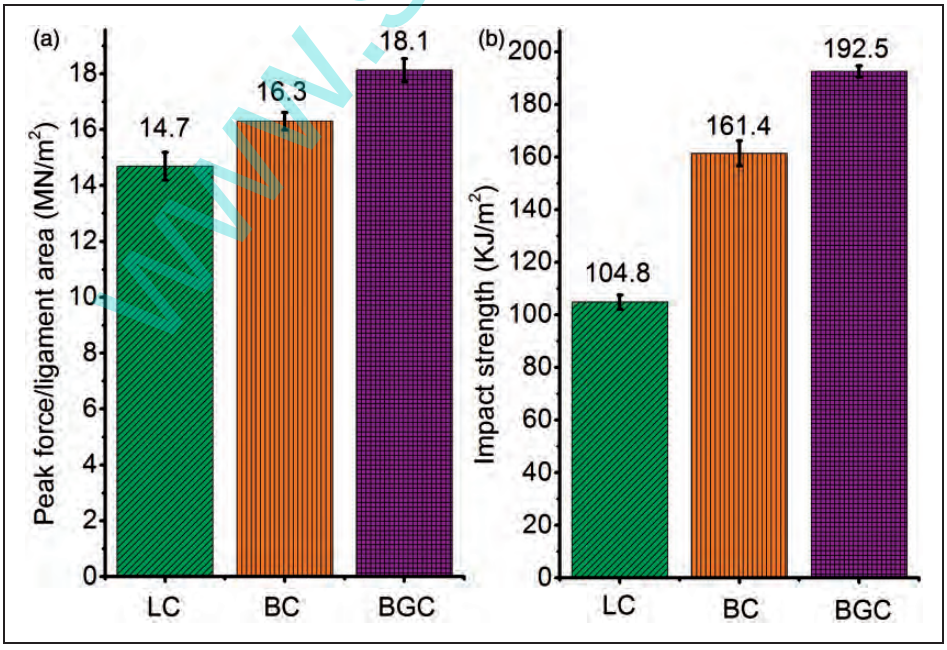

Figure 14. Peak force/ligament area (a) and impact strength (b) for the three unaged composites.

www.spm.com.cn

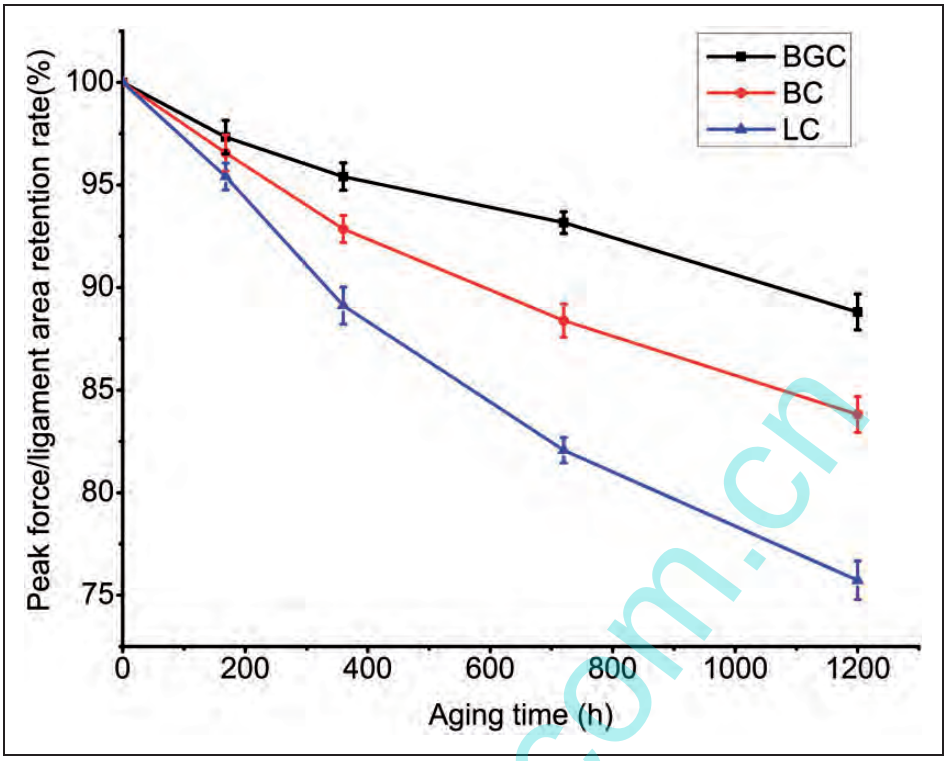

Figure 15. Effect of aging time on maximum peak force per ligament area for the three composites aged at 140°C.

broken fibers on the compression surface but none on the tension surface (Figure 13(b)). Furthermore, the delamination was prevented effectively by the braider yarns in the thickness direction of the braided preform, so there was no delamination (the side surface in Figure 13(b)). As the near net shape structure played an important role in preventing the propagation of the cracks, absorbing most of energy, the F_{max} and impact strength of BC were higher than those of LC. The F_{max} and impact strength retention rates of BGC, which increased by 11% and 19.3%, respectively, compared to those of BC, could be attributed to the reinforcing effect of the GN-reinforced gradient interphase layer. The interfacial reinforcing mechanism by the GN might be summarized as follows: (1) the stiffness of gradient interphase was lower than that of carbon fiber and higher than that of epoxy. The gradient stiffness made the gradient interphase act as a stress transfer medium and the load can be transferred from epoxy to carbon fibers uniformly; (2) GN had a rough and wrinkled surface topology that can enable it to mechanically interlock, increasing the interfacial friction and restricting the movement of the different phase of the materials at the composite interface; (3) GN produced by thermal reduction of GO[25] has residual hydroxyl and epoxide functional groups that could interact covalently with the epoxy chains thereby further promoting interfacial adhesion.

In order to compare the thermo-oxidative stability of the three composites, the normalized method was used to analyze the F_{max} and impact strength data. Figures 15 and 16 show the F_{max} and impact strength retention rates of the three composites after thermo-oxidative aging, respectively. It can be seen that the F_{max} and the impact strength retention rates of the three composites decreased with the increasing of aging time. After aging for 1200 h, the F_{max} retention rate of LC, BC, and BGC was 75.7%, 83.8%, and 88.8%, respectively. The corresponding impact strength retention rate of LC, BC, and BGC was 85.9%, 90.8%, and 93.9%, respectively. The decreases should be attributed to the progressive deterioration of the matrix and fiber–matrix interface caused by thermo-oxidative aging. Because of the matrix degradation, the resistance of the specimen to failure (by denting and compression) at the point of impact was reduced, and also because of the weak interface, the load transfer from the matrix to the fibers was not effective. By comparing LC and BC, the F_{max} and impact strength retention rates of BC were higher than those of LC. After aging for 1200 h, the F_{max} and impact strength retention rates of BC were 8% and 5% higher than those of LC, respectively. One reason was that the LC lost more weight than that of BC, and the extra weight loss was caused by the fiber–matrix interface oxidation. Therefore, interface of LC

www.sgm.com.cn

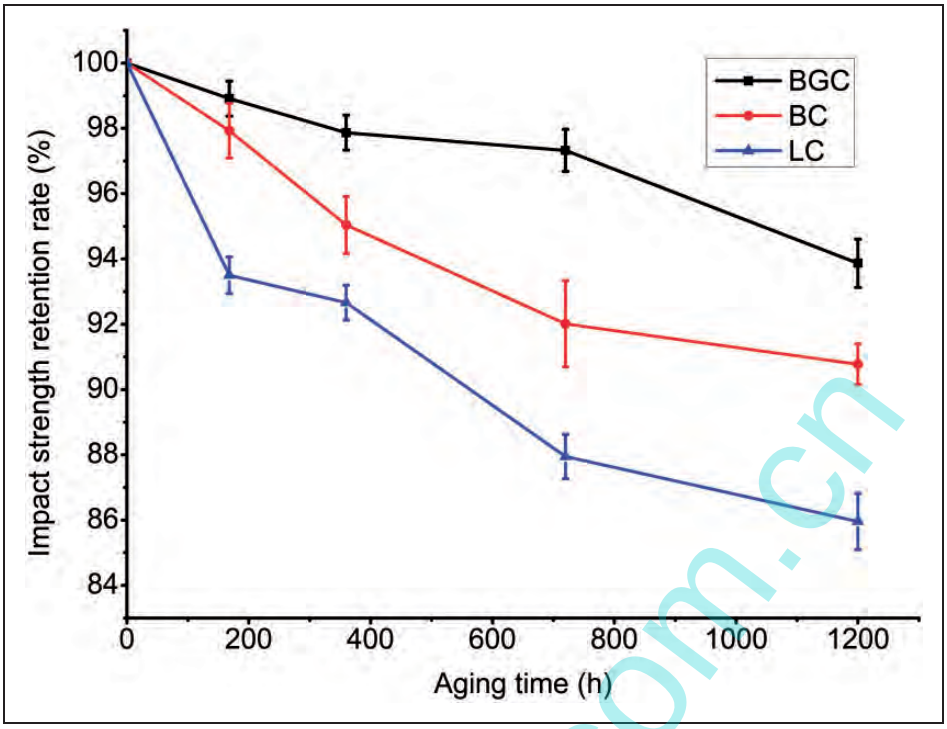

Figure 16. Effect of aging time on impact strength for the three composites aged at 140°C.

was damaged more seriously than that of BC at the same aging condition. The weak fiber–matrix interface can accelerate the oxidative degradation of CFPMCs. Another reason was that the micro-cracks were easily produced at the ply interfaces of LC specimens due to anisotropy of oxidation diffusion. The micro-cracks were prone to progress along the layer-to-layer interface when the LC specimens suffered impact loads and finally leading to delamination. This phenomenon would be exacerbated when the resin was damaged and the adhesive force between fiber bundles and resin decreased after thermo-oxidative aging. On the contrary, all braided yarns of BC interweave together forming a fully integrated structure (Figure 2(c)), which can enable it to mechanically interlock, even if the cracks are formed at the interlaced places of braided yarns, they will be hindered by the neighboring braided yarns. Therefore, the integrated structure of BC had more effective ability to make fibers bear impact loads together although the resin was damaged and the adhesive force between fiber bundles and resin decreased after thermo-oxidative aging. The F_{max} and impact strength retention rates of BGC were 5% and 3% higher than those of BC, respectively. According to the weight loss, the photomicrographs and the SEM analyses, it can be believed that GN-reinforced gradient interface layer provided an effective shield against the degradation of the fiber–matrix interface. The effect for GN is likely due to several reasons: (1) GN produced by thermal reduction of GO[25] has residual hydroxyl and epoxide functional groups, which could interact covalently with the epoxy chains thereby further promoting interfacial adhesion, which can prevent oxygen penetrate deep into the composite along the fiber–matrix interface during the aging process, reducing the interface oxidation; (2) the thermal conductivity of the GN-reinforced gradient interphase layer was lower than that of carbon fiber and higher than that of matrix. The gradient conductive layer might transfer the interfacial thermal stress, mitigating the interface damage; (3) the rough and wrinkled surface topology of GN can enable it to mechanically interlock, restricting the movement of the different phase of the materials at the composite interface although the adhesive force between fiber bundles and resin decreased after long time accelerated aging at high temperature.

After exposure to 140°C for 1200 h, the F_{max} and impact strength retention rates of BGC were 13% and 8% higher than those of LC, respectively. The results suggested that the 3D-4Dir braided structure and GN-reinforced gradient interface exhibited synergetic reinforcing effect on thermo-oxidative stability of CFPMCs.

Conclusions

This paper investigated the effects of reinforced structure (3D-4Dir braiding preform and laminated plain woven fabric) and GN-reinforced hierarchical interface on the impact properties of CFPMCs before and after thermo-oxidative aging. Before aging, the F_{max} and impact

www.spm.com.cn

strength of BC increased by 11% and 54%, respectively, compared with those of LC. It was because the near net shape structure of BC can prevent the propagation of the cracks and resist delamination damage. The F_{max} and impact strength retention rates of BGC increased by 11% and 19.3%, respectively, compared with those of BC. It was related to the fact that the GN-reinforced gradient interphase may transfer stress from epoxy to carbon fiber uniformly, restrict the movement of the different phase of the materials at the interface, and promote interfacial adhesion. After exposure to 140°C, the impact properties of the three composites decreased with the increase of aging time due to the deterioration of the matrix and fiber–matrix interface, in the form of weight loss, micro-cracks, and fiber/matrix debonding. After aging for 1200 h, the F_{max} and impact strength retention rates of BC were 8% and 5% higher than those of LC, respectively. There were two reasons that account for this phenomenon. First of all, the LC specimens, having four times higher quantity of fibers open ends, had shown 1.3 times the weight loss compared to the BC specimens. As the higher weight loss was due to interface oxygenation, the fiber–matrix interface of LC was damaged more seriously than that of BC at the same aging condition. Last but not the least, the integrated structure of 3D-braided composite can make the fibers bear impact load together and resist delamination damage although the matrix and interface properties decreased after longtime thermo-oxidative aging. The F_{max} and impact strength retention rates of BGC were 5% and 3% higher than those of BC, respectively. It was because the GN-reinforced gradient interphase may provide an effective shield against interface oxidation, transfer the interfacial thermal stress, and restrict the movement of the different phase of the materials at the composite interface. Compared with LC, the F_{max} and impact strength retention rates of BGC were 13% and 8% higher than those of LC, respectively. These results demonstrated that the 3D-4Dir braided structure and GN-reinforced gradient interface have an obvious synergetic reinforcing effect on the impact performance of CFPMCs, which provides an easy and effective way to design and improve the durability, safety, and reliability of CFPMCs that are increasing the material of choice in the aerospace industry.

Conflict of interest

None declared.

Funding

The authors wish to acknowledge the sponsorship of Tianjin Municipal Science and Technology Commission, China (Nos. 10SYSYJC27800 and11ZCKFSF00500).

References

1. Yang XL, Wang ZC, Xu MZ, et al. Dramatic mechanical and thermal increments of thermoplastic composites by multi-scale synergetic reinforcement: carbon fiber and graphene nanoplatelet. *Mater Des* 2013; 44: 74–80.
2. Zhang C, Binienda WK, Morscher GN, et al. Experimental and FEM study of thermal cycling induced microcracking in carbon/epoxy triaxial braided composites. *Compos Part A* 2013; 46: 34–44.
3. Rahmani H, Najafi SHM and Ashori A. Mechanical performance of epoxy/carbon fiber laminated composites. *J Reinforced Plast Compos* 2014; 33: 733–740.
4. Vu DQ, Gigliotti M and Lafarie-Frenot MC. The effect of thermo-oxidation on matrix cracking of cross-ply 0/90 (S) composite laminates. *Compos Part A* 2013; 44: 114–121.
5. Haque MH, Upadhyaya P, Roy S, et al. The changes in flexural properties and microstructures of carbon fiber bismaleimide composite after exposure to a high temperature. *Compos Struct* 2014; 108: 57–64.
6. Sarasini F, Tirillo J, Ferrante L, et al. Drop-weight impact behaviour of woven hybrid basalt-carbon/epoxy composites. *Compos Part B* 2014; 59: 204–220.
7. Solirnan EM, Sheyka MP and Taha MR. Low-velocity impact of thin woven carbon fabric composites incorporating multi-walled carbon nanotubes. *Int J Impact Eng* 2012; 47: 39–47.
8. Li DS, Fang DN, Zhang GB, et al. Effect of temperature on bending properties and failure mechanism of three-dimensional braided composite. *Mater Des* 2012; 41: 167–170.
9. Bowles KJ, Madhukar M, Papadopoulos DS, et al. The effects of fiber surface modification and thermal aging on composite toughness and its measurement. *J Compos Mater* 1997; 31: 552–579.
10. Yavari F, Rafiee MA, Rafiee J, et al. Dramatic increase in fatigue life in hierarchical graphene composites. *ACS Appl Mat Interf* 2010; 2: 2738–2743.
11. Zhang X, Fan X, Yan C, et al. Interfacial microstructure and properties of carbon fiber composites modified with graphene oxide. *ACS Appl Mat Interf* 2012; 4: 1543–1552.
12. Marcano DC, Kosynkin DV, Berlin JM, et al. Improved synthesis of graphene oxide. *ACS Nano* 2010; 4: 4806–4814.
13. Chen L, Jin H, Xu ZW, et al. A design of gradient interphase reinforced by silanized graphene oxide and its effect on carbon fiber/epoxy interface. *Mater Chem Phys* 2014; 145: 186–196.
14. Chen L. *The research of graphene irradiation modification and the interface mechanism of the carbon fiber/epoxy composites toughened by graphene and functionalized graphene*. PhD Thesis, Tianjin Polytechnic University, 2013.
15. Sun X and Sun CJ. Mechanical properties of three-dimensional braided composites. *Compos Struct* 2004; 65: 485–492.
16. Fan W and Li JL. Rapid evaluation of thermal aging of a carbon fiber laminated epoxy composite. *Polym Compos* 2014; 35: 975–984.

www.sagepub.com

17. Akhavan O, Ghaderi E and Rahighi R. Toward single-DNA electrochemical biosensing by graphene nanowalls. *Acs Nano* 2012; 6: 2904–2916.
18. Zhao F, Huang YD, Liu L, et al. Formation of a carbon fiber/polyhedral oligomeric silsesquioxane/carbon nanotube hybrid reinforcement and its effect on the interfacial properties of carbon fiber/epoxy composites. *Carbon* 2011; 49: 2624–2632.
19. Munz M, Sturm H, Schulz E, et al. The scanning force microscope as a tool for the detection of local mechanical properties within the interphase of fibre reinforced polymers. *Compos Part A* 1998; 29: 1251–1259.
20. Wu H and Drzal LT. Graphene nanoplatelet paper as a light-weight composite with excellent electrical and thermal conductivity and good gas barrier properties. *Carbon* 2012; 50: 1135–1145.
21. Polansky R, Mentlik V, Prosr P, et al. Influence of thermal treatment on the glass transition temperature of thermosetting epoxy laminate. *Polym Test* 2009; 28: 428–436.
22. Ohno S, Lee MH, Lin KY, et al. Thermal degradation of IM7/BMI5260 composite materials: characterization by X-ray photoelectron spectroscopy. *Mater Sci Eng A* 2000; 293: 88–94.
23. Schoeppner G, Tandon G and Ripberger E. Anisotropic oxidation and weight loss in PMR-15 composites. *Compos Part A* 2007; 38: 890–904.
24. Tandon GP and Ragland WR. Influence of laminate lay-up on oxidation and damage growth: isothermal aging. *Compos Part A* 2011; 42: 1127–1137.
25. Dikin DA, Stankovich S, Zimney EJ, et al. Preparation and characterization of graphene oxide paper. *Nature* 2007; 448: 457–460.
26. Madhukar MS, Bowles KJ and Papadopoulos DS. Thermo-oxidative stability and fiber surface modification effects on the inplane shear properties of graphite/PMR-15 composites. *J Compos Mater* 1997; 31: 596–618.
27. Schuster J, Heider D, Sharp K, et al. Thermal conductivities of three-dimensionally woven fabric composites. *Compos Sci Technol* 2008; 68: 2085–2091.

www.spm.com.cn